

## CHEMICAL COMPOSITION OF BRIGHT STARS IN THE CONTINUOUS VIEWING ZONE OF THE TESS SPACE MISSION

G. TAUTVAIŠIENĖ,<sup>1</sup> Š. MIKOLAITIS,<sup>1</sup> A. DRAZDAUSKAS,<sup>1</sup> E. STONKUTĖ,<sup>1</sup> R. MINKEVIČIŪTĖ,<sup>1</sup> H. KJELDSSEN,<sup>1,2</sup> K. BROGAARD,<sup>1,2</sup> C. VON ESSEN,<sup>1,2</sup> F. GRUNDAHL,<sup>1,2</sup> E. PAKŠTIENĖ,<sup>1</sup> V. BAGDONAS,<sup>1</sup> AND C. VISCASILLAS VÁZQUEZ<sup>1</sup>

<sup>1</sup>*Astronomical Observatory, Institute of Theoretical Physics and Astronomy, Vilnius University, Sauletekio av. 3, 10257 Vilnius, Lithuania*

<sup>2</sup>*Stellar Astrophysics Centre, Department of Physics and Astronomy, Aarhus University, Ny Munkegade 120, DK-8000 Aarhus C, Denmark*

(Received 2019 December 16; Revised 2020 April 6; Accepted 2020 April 18)

Submitted to ApJS

### ABSTRACT

Accurate atmospheric parameters and chemical composition of stars play a vital role in characterizing physical parameters of exoplanetary systems and understanding of their formation. A full asteroseismic characterization of a star is also possible if its main atmospheric parameters are known. The NASA Transiting Exoplanet Survey Satellite (TESS) space telescope will play a very important role in searching of exoplanets around bright stars and stellar asteroseismic variability research. We have observed all 302 bright ( $V < 8$  mag) and cooler than F5 spectral class stars in the northern TESS continuous viewing zone with a 1.65 m telescope at the Molėtai Astronomical Observatory of Vilnius University and the high-resolution Vilnius University Echelle Spectrograph. We uniformly determined the main atmospheric parameters, ages, orbital parameters, velocity components, and precise abundances of 24 chemical species (C(C<sub>2</sub>), N(CN), [O I], Na I, Mg I, Al I, Si I, Si II, Ca I, Ca II, Sc I, Sc II, Ti I, Ti II, V I, Cr I, Cr II, Mn I, Fe I, Fe II, Co I, Ni I, Cu I, and Zn I) for 277 slowly rotating single stars in the field. About 83% of the sample stars exhibit the Mg/Si ratios greater than 1.0 and may potentially harbor rocky planets in their systems.

*Keywords:* High resolution spectroscopy; Catalogs; Chemical abundances.

### 1. INTRODUCTION

The NASA Transiting Exoplanet Survey Satellite (TESS) is an ongoing space mission with primary goal to search for planets in systems of bright and nearby stars (Ricker et al. 2015). The two-year mission is planned to observe southern and northern ecliptic hemispheres, each divided into 13 sectors. A total of 26 sectors will cover 85% of the sky. Those sectors in each hemisphere overlap at the ecliptic poles, forming circular regions – continuous viewing zones (CVZs). The CVZs will have an almost full year observing coverage; such an advantage would be significant in finding planets of longer orbital periods. The TESS mission at a 30 minute ca-

dence will observe all stars in its field of view, yet for more than 200,000 stars selected for a Candidate Target List (CTL), a two minute cadence will be used. A complex mechanism of CTL compilation is described in more detail in Stassun et al. (2018).

TESS was launched on 2018 April and has already finished its first year observations of the southern ecliptic hemisphere and now is pointing to sectors of the northern ecliptic hemisphere. As of 2019 December, TESS mission results are 37 confirmed planets and 1417 planet candidates (NASA exoplanet archive; Akesson et al. 2013). However, the former number will likely be increased, since Barclay et al. (2018) estimated that  $1250 \pm 70$  exoplanets will be found using the two minute cadence mode and 3100 and 10,000 exoplanets – using the 30 minute cadence mode around bright dwarfs and fainter stars, respectively.

Since objects of the TESS mission are much nearer and 10–100 times brighter than those of the Kepler mission (Borucki et al. 2010; Koch et al. 2010), they are excellent targets for ground-based observations (Ricker et al. 2015; Barclay et al. 2018). Data from ground-based observations are a crucial ingredient in order to characterize identified exoplanets and especially their atmospheres. The chemical composition of the protoplanetary disk and planet formation pathways are linked to the bulk composition of the parent star. Furthermore, different stellar Galactic subcomponents could produce planets with different properties. Thus, it becomes crucial to determine the bulk chemical composition of the stars in different Galactic populations. The homogeneously determined detailed stellar abundances from ground-based observations are starting to be transferred to the models that help to deduce properties of planet building blocks and exoplanets themselves (see e.g., Santos et al. 2017; Cabral et al. 2019; Bitsch & Battistini 2020). Moreover, TESS is expected to deliver major improvements in characterizing planets. Different from the Kepler mission (Thompson et al. 2018), due to the large signal-to-noise ratio (S/N) of TESS planet candidates, the atmospheric characterization of Neptune and Earth-sized planets will be feasible with current and future technology and amenable for some hundreds of them (Kempson et al. 2018).

Since only around one third of bright ( $V < 8$  mag) stars have high-resolution spectroscopic studies, in 2016, we started a Spectroscopic and Photometric Survey of bright stars in the northern hemisphere. In papers by Mikolaitis et al. (2018, hereafter M18) and Mikolaitis et al. (2019, hereafter M19), we published atmospheric parameters and detailed chemical compositions for 249 bright dwarf stars located in two preliminary ESA PLATO fields: STEP02 and NPF (Rauer et al. 2014, 2016). With the current work, we aimed to observe high-resolution spectra for all both dwarf and giant stars with  $V < 8$  mag and cooler than F 5 spectral type in the TESS northern CVZ and to determine homogeneously their main parameters and detailed chemical compositions. We hope our work will be useful in characterizing exoplanets potentially discovered by TESS around those stars and for the asteroseismic stellar analyses.

## 2. OBSERVATIONS AND METHOD OF ANALYSIS

### 2.1. Target Selection and Observations

Having our observational possibilities and methods of analysis developed in mind, we decided to observe high-resolution spectra of all bright ( $V < 8$  mag) F5 and cooler stars ( $T_{\text{eff}} < 6500$  K) in the whole TESS northern

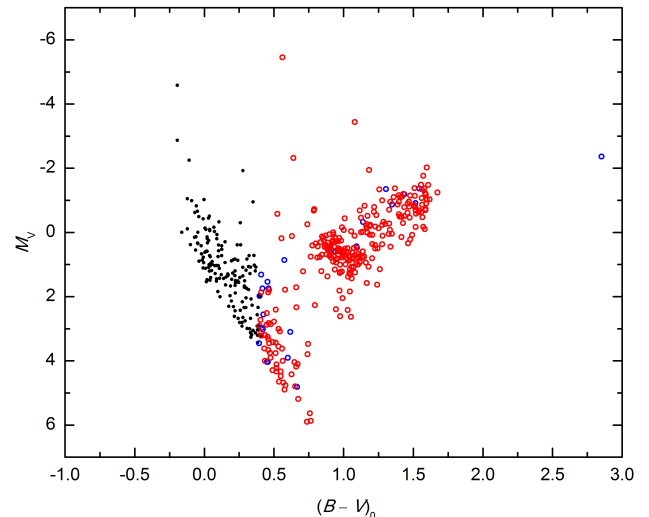


**Figure 1.** Colormagnitude diagram of stars in the investigated TESS CVZ field. The FGK spectral type stars investigated in this work are marked as open circles; objects with determined parameters are indicated as red circles and the peculiar stars as blue circles.

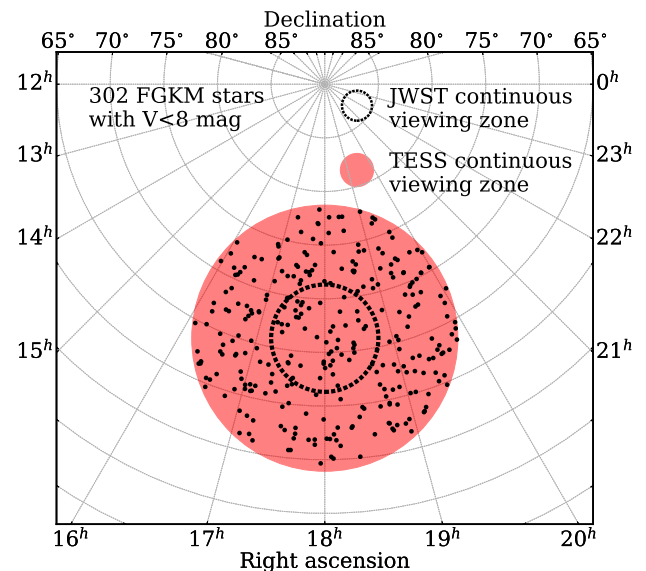


**Figure 2.** Positions (R.A. and decl. in hours and degrees, respectively) of the program stars (black dots). The CVZs of TESS and JWST are marked as well.

CVZ which is a region around the northern ecliptic pole with a diameter of around 24 degrees.

We examined a color-magnitude diagram of all  $V < 8$  mag and  $(B - V) > 0.39$  mag stars in the selected field (Figure 1). In M18, we showed that  $T_{\text{eff}} < 6500$  K corresponds to approximately  $(B - V) > 0.39$  mag. In this way, we found 302 stars in the selected field that met these criteria (see Figure 2) and we have observed all of them during the period of 2018–2019. Of the observed

stars, 53 fall within the 5 degree radius CVZ of the upcoming James Webb Space Telescope (JWST) mission (Gardner et al. 2006).

We used the 1.65 m telescope at the Moletai Astronomical Observatory of Vilnius University in Lithuania that is equipped with the high-resolution Vilnius University Echelle Spectrograph (VUES; Jurgenson et al. 2016). This spectrograph has a wavelength coverage from 400 to 900 nm in  $R \sim 36,000$ ,  $\sim 51,000$ , and  $\sim 68,000$  resolution modes. For our work, we used the  $\sim 68,000$  resolution mode for the M spectral type stars and the  $\sim 36,000$  resolution mode for other objects. Exposure times varied between 900 and 2400 s and S/Ns varied between 75 and 200 with the median value at 96, depending on stellar magnitudes. The VUES data reduction was accomplished on the site using an automated pipeline described by Jurgenson et al. (2016).

### 2.2. Radial Velocity Determination and Identification of Double-line Binaries and Fast-rotating Stars

For an initial spectral analysis, we used the standard cross-correlation function (CCF) method to obtain spectroscopic radial velocity values. The CCF revealed 11 double-line binaries and 10 fast-rotating stars, which we postponed for a further analysis. Figure 3 shows the CCF examples. It was not possible to measure equivalent widths of lines for those fast-rotating stars with a satisfactory quality because of the broad and blended lines. The classical equivalent width method that we used to determine the main stellar atmospheric parameters could not be applied to the fast-rotating stars with strongly broadened and diminished lines. From the subsequent analysis, we also excluded the four coolest stars (see Section 2.3) with severe line-blending. In this way, 277 stars filled our final sample of the present analysis.

### 2.3. Stellar Atmospheric Parameters and Chemical Composition

In order to determine the main stellar atmospheric parameters (effective temperature,  $T_{\text{eff}}$ ; surface gravity,  $\log g$ ; microturbulence velocity,  $v_t$ ; and metallicity  $\langle [\text{Fe}/\text{H}] \rangle$ ), we adopted a classical method of equivalent widths of atomic neutral and ionized iron lines. We used a combination of the DAOSPEC (Stetson & Pancino 2008) and MOOG (Sneden 1973) codes the same way as the Vilnius node was using in the *Gaia*-ESO Survey (see Smiljanic et al. 2014 and M18).

Detailed abundances of 24 chemical species were determined applying a spectral synthesis method with the TURBOSPECTRUM code (Alvarez & Plez 1998). The spectral analysis was done using a grid of MARCS stellar atmosphere models (Gustafsson et al. 2008) and the

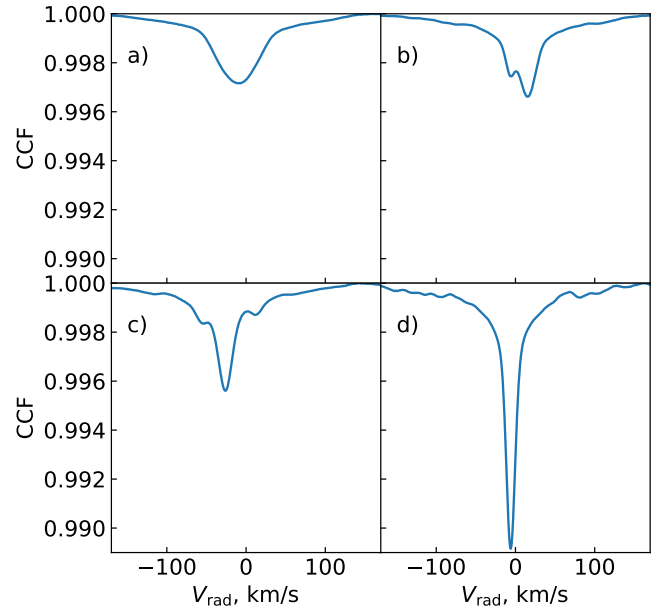


**Figure 3.** Examples of CCFs produced for calculating the radial velocities and detection of double-line binary stars: (a) the fast-rotating star HD 155513, (b) the double-line spectroscopic binary HD 180160, (c) HD 160780 showing three profiles, and (d) a typical slow-rotating star HD 149843.

Solar abundances by Grevesse et al. (2007). Atomic lines were selected from the *Gaia*-ESO line-list by Heiter et al. (2015). We have also used the molecular line lists:  $\text{C}_2$  (Brooke et al. 2013; Ram et al. 2014); CN (Sneden et al. 2014); CH (Masseron et al. 2014); SiH (Kurucz 1993); FeH (Dulick et al. 2003); CaH (B. Plez, private communication); and OH, MgH, NH (T. Masseron, private communication). For the carbon abundance determination, we used two regions: the  $\text{C}_2$  Swan (1, 0) band head at 5135 Å and the  $\text{C}_2$  Swan (0, 1) band head at 5635 Å. For the nitrogen abundance determination, we used  $^{12}\text{C}^{14}\text{N}$  molecular lines in the region 7980–8005 Å. The oxygen abundance was determined from the forbidden [O I] line at 6300 Å. These elements require a more detailed analysis, as they are bound by the molecular equilibrium. First, we performed a couple of iterations until the determinations of carbon and oxygen abundances converged. After that, we used both carbon and oxygen values to determine the abundance of nitrogen.

For more details of the chemical composition analysis, we refer to our recent studies (M19; Stonkutė et al. 2020).

The applied method did not work for four M3 and cooler stars: V\* HW Dra, V\* GP Dra, and V\* TX Dra are M3–M5 type stars with *Gaia* DR2  $T_{\text{eff}} \approx 3300$  K; a specific analysis is also needed for V\* UX Dra which

is classified as a C-N5 carbon star with  $T_{\text{eff}} \approx 2817$  K (Lambert et al. 1986).

#### 2.4. Stellar Ages

To calculate the stellar ages, and their errors, we used the code UniDAM (the unified tool to estimate distances, ages and masses) by Mints & Hekker (2017). The code uses a Bayesian approach and the PARSEC isochrones (Bressan et al. 2012). As an input, we used the stellar atmospheric parameters determined in this work together with the  $J$ ,  $H$ , and  $K$  magnitudes from the the Two Micron All-Sky Survey (2MASS) (Skrutskie et al. 2006) and the  $W1$  and  $W2$  magnitudes from AllWISE (Cutri & et al. 2014).

Crossmatching of our sample stars with the 2MASS and AllWISE catalogs provided us data for 273 stars that had entries in at least one infrared photometry study: 198 stars had magnitudes from both, and 75 had magnitudes from 2MASS. After calculating the ages, we discarded 59 stars that had flags reported after calculation that meant either unreliable photometry, or the result being off the model grid, or just an unreliable determination (see Section 6.1 in Mints & Hekker 2017 for more interpretations). Finally, we were left with 214 stars for which we report the derived ages in this work.

#### 2.5. Kinematic Properties

The main kinematic parameters ( $R_{\text{mean}}$ ,  $z_{\text{max}}$ ,  $e$ ,  $U$ ,  $V$ , and  $W$ ) for the stars were calculated using the python-based package for galactic-dynamics calculations *galpy*<sup>1</sup> by Bovy (2015). The parallaxes, proper motions, and coordinates required for *galpy* were taken from the *Gaia* data release 2 (DR2) catalog (Luri et al. 2018; Katz et al. 2019).

The *galpy* was set to integrate orbits for 5 Gyr. Observational errors were estimated using 1000 Monte Carlo calculations according to the errors in the input parameters. The position and movement of the Sun are those from Bovy et al. (2012) ( $R_{\text{gc}\odot} = 8$  kpc and  $V_{\odot} = 220$  km s<sup>-1</sup>), the distance from the Galactic plane  $z_{\odot} = 0.02$  kpc (Joshi 2007), and the LSR from Schönrich et al. (2010) ( $U$ ,  $V$ ,  $W = 11.1, 12.24, 7.25$  km s<sup>-1</sup>).

#### 2.6. Errors on Atmospheric Parameters and Abundances

The errors on the atmospheric parameters were estimated as follows:

- We tested the sensitivity of computed atmospheric parameters to the quality of the spectra. As a rep-

<sup>1</sup> <http://github.com/jobovy/galpy>

**Table 1.** Errors Due to the Uncertain Continuum Placement and Equivalent width Measurement, Based on the Monte Carlo Simulations.

	S/N=25	S/N=50	S/N=75
TYC 3910-1710-1			
$T_{\text{eff}} = 4458$ K, $\log g = 2.72$ , $[\text{Fe}/\text{H}] = -0.14$			
$\sigma_{T_{\text{eff}}}$	49	45	32
$\sigma_{\log g}$	0.09	0.09	0.09
$\sigma_{[\text{Fe}/\text{H}]}$	0.03	0.03	0.01
$\sigma_{v_t}$	0.08	0.08	0.04
Na I	0.08	0.08	0.05
Mg I	0.10	0.06	0.03
Al I	0.09	0.07	0.04
Si I	0.05	0.04	0.03
Si II	0.08	0.08	0.05
Ca I	0.10	0.07	0.05
Ca II	0.09	0.08	0.07
Sc I	0.12	0.08	0.06
Sc II	0.11	0.11	0.06
Ti I	0.10	0.08	0.06
Ti II	0.11	0.09	0.03
V I	0.09	0.08	0.06
Cr I	0.09	0.09	0.05
Cr II	0.12	0.09	0.05
Mn I	0.10	0.08	0.06
Fe I	0.09	0.06	0.04
Fe II	0.13	0.09	0.07
Co I	0.09	0.07	0.01
Ni I	0.06	0.05	0.02
Cu I	0.07	0.06	0.06
Zn I	0.12	0.09	0.06

resentative star for this test, we choose TYC 3910-1710-1 – a giant star with high signal-to-noise spectra. We artificially degraded the spectra of this star to S/Ns of 25, 50, and 75 per pixel and determined its atmospheric parameters. Of the randomly degraded spectra for each S/N, 100 were used and the generated statistics are presented in Table 1. The same test for dwarf stars was shown in M18.

- The uncertainties in the atomic parameters of the used lines create a scatter of measured iron abundances and also an error in a linear regression fit that can be directly propagated to follow the uncertainties of atmospheric parameters. Therefore, the uncertainties for each of the main atmospheric parameters are provided for every star in machine-readable Table A1 and they are

**Table 2.** Median Effects on the Derived Abundances Resulting from the Atmospheric Parameter Uncertainties for the Sample Stars.

El	$\Delta T_{\text{eff}}$ K	$\Delta \log g$	$\Delta[\text{Fe}/\text{H}]$	$\Delta v_t$ $\text{km s}^{-1}$	$\sigma_{\text{scat}}^a$	$N_{\text{max}}^b$	$\sigma_{\text{total}}^c[\frac{\text{El}}{\text{H}}]$	$\sigma_{\text{all}}^d[\frac{\text{El}}{\text{H}}]$
C (C <sub>2</sub> )	0.00	0.03	0.01	0.01	0.02	2	0.03	0.04
N (CN)	0.06	0.05	0.01	0.01	0.05	7	0.08	0.08
O ([O I])	0.01	0.08	0.07	0.00	0.06	1	0.11	0.13
Na I	0.00	0.03	0.02	0.02	0.03	4	0.05	0.05
Mg I	0.01	0.07	0.02	0.03	0.06	5	0.08	0.12
Al I	0.01	0.02	0.03	0.03	0.04	5	0.03	0.07
Si I	0.01	0.02	0.02	0.02	0.03	14	0.02	0.03
Si II	0.01	0.05	0.01	0.02	0.07	7	0.06	0.10
Ca I	0.02	0.07	0.02	0.02	0.06	31	0.08	0.10
Ca II	0.03	0.06	0.02	0.04	0.05	7	0.07	0.09
Sc I	0.04	0.03	0.02	0.03	0.08	7	0.05	0.11
Sc II	0.02	0.08	0.02	0.04	0.03	12	0.10	0.10
Ti I	0.04	0.04	0.01	0.02	0.03	81	0.07	0.08
Ti II	0.01	0.08	0.04	0.04	0.04	19	0.09	0.09
V I	0.03	0.01	0.02	0.04	0.05	8	0.05	0.07
Cr I	0.02	0.03	0.02	0.03	0.05	21	0.05	0.06
Cr II	0.02	0.08	0.02	0.04	0.03	2	0.10	0.11
Mn I	0.03	0.03	0.02	0.04	0.05	14	0.05	0.07
Fe I	0.02	0.03	0.02	0.03	0.05	138	0.05	0.06
Fe II	0.01	0.08	0.03	0.04	0.04	11	0.09	0.12
Co I	0.01	0.01	0.01	0.02	0.05	7	0.02	0.07
Ni I	0.01	0.02	0.01	0.04	0.03	30	0.03	0.07
Cu I	0.03	0.02	0.02	0.02	0.05	6	0.04	0.06
Zn I	0.01	0.02	0.02	0.02	0.09	3	0.04	0.11

Notes.

<sup>a</sup> $\sigma_{\text{scat}}$  stands for the median line-to-line scatter.

<sup>b</sup> $N_{\text{max}}$  presents the number of lines investigated.

<sup>c</sup> $\sigma_{\text{total}}([\text{El}/\text{H}])$  stands for the median of the quadratic sum of all four effects on  $[\text{El}/\text{H}]$ .

<sup>d</sup> $\sigma_{\text{all}}([\text{El}/\text{H}])$  is a median of the combined effect of  $\sigma_{\text{total}}([\text{El}/\text{H}])$  and the line-to-line scatter  $\sigma_{\text{scat}}$ .

computed the same way as published in the description of the *Gaia*-ESO Vilnius node by [Smiljanic et al. \(2014\)](#). The median errors measured by the algorithm in the full stellar sample are  $\sigma_{T_{\text{eff}}}=60$  K,  $\sigma_{\log g}=0.21$  dex,  $\sigma_{[\text{Fe}/\text{H}]}=0.11$  dex, and  $\sigma_{v_t}=0.23$   $\text{km s}^{-1}$ .

We have made several tests to understand the error budget in our chemical abundance measurements:

- We used the same 300 generated spectra of the giant star TYC 3910-1710-1 for three S/N values to measure abundances in order to estimate their sensitivity to quality of the spectrum. These results are provided in Table 1. The same test for dwarf stars was accomplished in [M19](#).

- Evaluation of the line-to-line scatter is a way to estimate random errors if the number of lines is large enough. A median of the standard deviation for a given element,  $\sigma_{\text{scat}}^*$ , is presented in the sixth column of Table 2.

- The uncertainties of the main atmospheric parameters were propagated into the errors of chemical abundances. The median errors of this type over the stellar sample are provided in Table 2.

The final error for every element for every star that is given in machine-readable Table A1 is a quadratic sum of effects due to uncertainty in four atmospheric parameters and the abundance scatter given by the lines.

In Section 3.6 of [M19](#), we have discussed that it should be safe to use the classical LTE approach to compute ele-



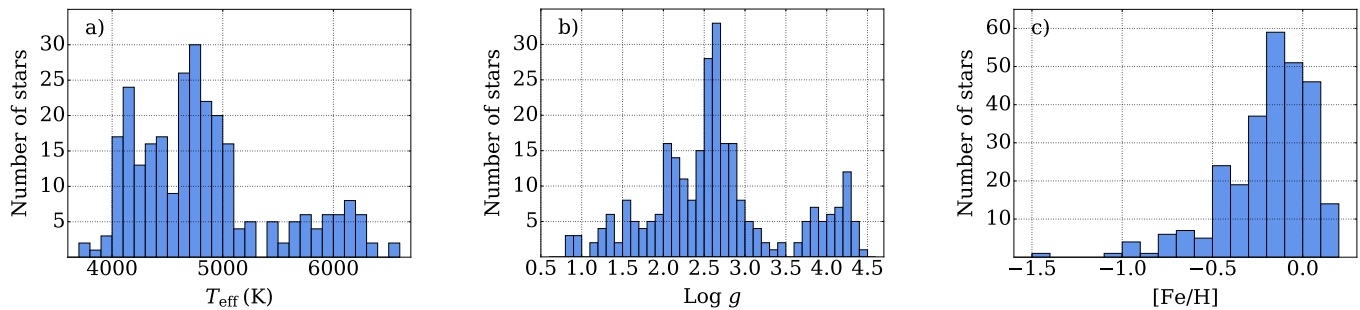


**Figure 4.** Histograms of the determined spectroscopic parameters ( $T_{\text{eff}}$ ,  $\log g$ , and  $[\text{Fe}/\text{H}]$ ) for the sample stars.

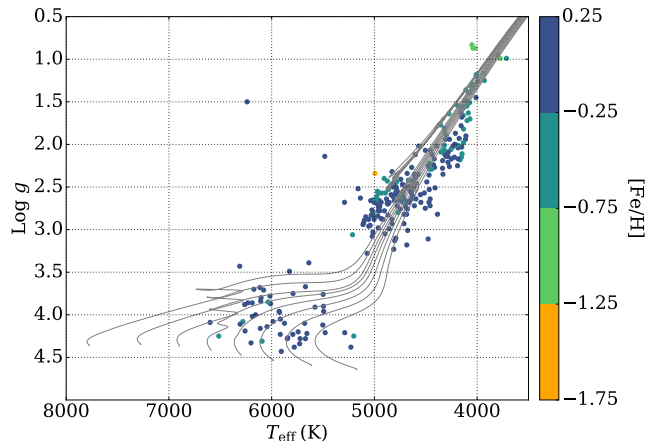


**Figure 5.**  $\log g$  and  $T_{\text{eff}}$  diagram of the investigated stars (dots) with metallicity coded by color. Evolutionary sequences by Bressan et al. (2012) with masses between 0.8 and  $1.5 M_{\odot}$  and  $Z_{\text{ini}} = 0.01$  are plotted as gray solid lines.

mental abundances in the metallicity regime of our sample stars. The NLTE effects for the majority of elemental abundances in our sample are negligible; the NLTE corrections were adopted just for the potassium abundances as they were determined from the large 7698.9 Å line. For manganese and copper, we have accounted for a hyperfine splitting as described in M19.

Since abundances of C, N, and O are bound together by the molecular equilibrium in the stellar atmospheres, we investigated how an error in one of them typically influences the abundance determination of another. We determined that  $\Delta[\text{O}/\text{H}] = 0.10$  causes  $\Delta[\text{C}/\text{H}] = 0.02$  and  $\Delta[\text{N}/\text{H}] = 0.04$ , and  $\Delta[\text{C}/\text{H}] = 0.10$  causes  $\Delta[\text{N}/\text{H}] = 0.11$  and  $\Delta[\text{O}/\text{H}] = 0.02$ , while  $\Delta[\text{N}/\text{H}] = 0.10$  has no effect on either the carbon or the oxygen abundances.

### 3. RESULTS AND DISCUSSION

The initial CCF analysis of spectra revealed 11 double- or even triple-line stellar systems. Of the 11, four are known spectroscopic binaries: HD 155902, HD 165700,  $\chi$  Dra, and HD 180160 (Nordström et al. 2004). The newly detected double-line spectroscopic binaries are the following stars: HD 152274, HD 145222, HD 170527,

HD 184756, and V\* AZ Dra, while the triple-line spectrum was found for HD 165988 and HD 160780. Of the stars, 10 appeared to be quite fast rotating ( $V_{\text{rot}} \geq 20 \text{ km s}^{-1}$ ): HD 161128, HD 164983, HD 179729, HD 171044, HD 238865, HD 173605, V\* omi Dra, HD 155513, HD 164330, and HD 165522. These stars were postponed for a further investigation requiring different methods of analysis and additional photometric and spectral observations. And finally, four stars had too low effective temperatures for our method of analysis and also will be investigated later. Thus, a full characterization was performed for a sample of the remaining 277 stars.

#### 3.1. Atmospheric Parameters and Elemental Abundances

Our sample of 277 slowly rotating stars have  $T_{\text{eff}}$  between 3700 and 6600 K with a peak at 4700 K,  $[\text{Fe}/\text{H}]$  are from  $-1.5$  dex to 0.25 dex with a peak at  $-0.25$  dex, and  $\log g$  are from 0.8 to 3.5 with a peak at 2.7 for giants and from 3.6 to 4.5 with a peak at 4.3 for dwarfs (more detailed distributions are presented in Figure 4). A  $\log g$  versus  $T_{\text{eff}}$  diagram of the stars colored according to their metallicity is presented in Figure 5.

From the *fe.h* catalog of the SIMBAD (Wenger et al. 2000) database and the PASTEL catalog (Soubiran et al. 2010) we found that there are only few studies that have derived stellar parameters for some stars of our sample. We have only 47 stars that were observed before with atmospheric parameters delivered using high-resolution spectrographs. This spectroscopic comparison sample is collected from McWilliam (1990); Hekker & Meléndez (2007); Luck & Heiter (2007); da Silva et al. (2011); Lee et al. (2011); Pompéia et al. (2011); Britavskiy et al. (2012); Afşar et al. (2012); Roederer et al. (2014); Liu et al. (2014); Adamczak & Lambert (2014); da Silva et al. (2015); Maldonado & Villaver (2016); Brewer et al. (2016); Jönsson et al. (2017); Luck (2017); Aguilera-Gómez et al. (2018); Deka-Szymankiewicz et al. (2018). The effective temperature and surface gravity consistency between our sample and the spectroscopic com-

parison sample of 47 stars are quite good:  $\langle \Delta T_{\text{eff}} \rangle = -11 \pm 58$  K and  $\langle \Delta \log g \rangle = -0.02 \pm 0.18$ .

We found 18 stars in common with the near-infrared, large-scale, stellar spectroscopic survey APOGEE 16th data release (DR16) (Ahumada et al. 2019). For the comparison, we were using calibrated parameters and abundances determined with the APOGEE Stellar Parameters and Chemical Abundance Pipeline (ASPCAP) (García Pérez et al. 2016). The biases for the main stellar atmospheric parameters from our sample are  $\langle \Delta T_{\text{eff}} \rangle = -48 \pm 47$  K and  $\langle \Delta \log g \rangle = 0.06 \pm 0.18$  dex. In Figure 6, we show a comparison of [Element/H] abundances for up to 18 stars in common with the APOGEE DR16. The average differences for all stars and standard deviations are calculated as our values minus the comparison values. The sample of common stars is not large; however, as one can see, the agreement for the majority of elements is very good. Regarding the C, N, and O elements, the APOGEE survey uses the infrared lines of CH, CN, and OH molecules, respectively, and the agreement for the carbon and oxygen abundances is quite good. The differences of 0.2 dex are between nitrogen and also of manganese abundances. As was shown in Smith et al. (2013, see their Figure 4), the larger Mn abundances in the APOGEE survey could be caused by a blending of the CN bands. The nitrogen abundance values are accumulating uncertainties of carbon and oxygen abundance determinations apart of others, thus they can be larger than for other chemical elements.

We find a similar  $T_{\text{eff}}$  bias if we compare our sample with the *Gaia* DR2 data.  $\langle \Delta T_{\text{eff}} \rangle = -62 \pm 99$  K for all 277 stars. The APOGEE and *Gaia* DR2  $T_{\text{eff}}$  bias is similar probably because the *Gaia* DR2  $T_{\text{eff}}$  data was taken from the Astrophysical Parameters Inference System (Apsis; Andrae et al. 2018) which was trained on a number of samples where the APOGEE giant star input was one of the dominant ones.

In Table A1, columns 29–76 contain relative to Solar abundances and uncertainties of C(C<sub>2</sub>), N(CN), [O I], Na I, Mg I, Al I, Si I, Si II, Ca I, Ca II, Sc I, Sc II, Ti I, Ti II, V I, Cr I, Cr II, Mn I, Fe I, Fe II, Co I, Ni I, Cu I, and Zn I for the 277 stars investigated in the present study. The abundances are presented in [Element/H] form. The [Fe I/H] and [Fe II/H] values occupy 77–80 columns of Table A1. All elemental abundance ratios with respect to [Fe I/H] are show in Figures 7 and 8 where the stars are colored according to their attribution to the Galactic subcomponents. The stellar attribution to subcomponents is presented in the column 83 of Table A1 and is described in the next section.

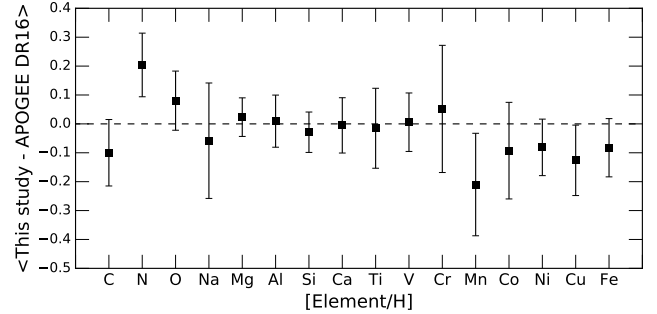


**Figure 6.** Comparison of abundances for up to 18 stars that we have in common with APOGEE DR16. The average differences and standard deviations are calculated as our values minus the comparison values.

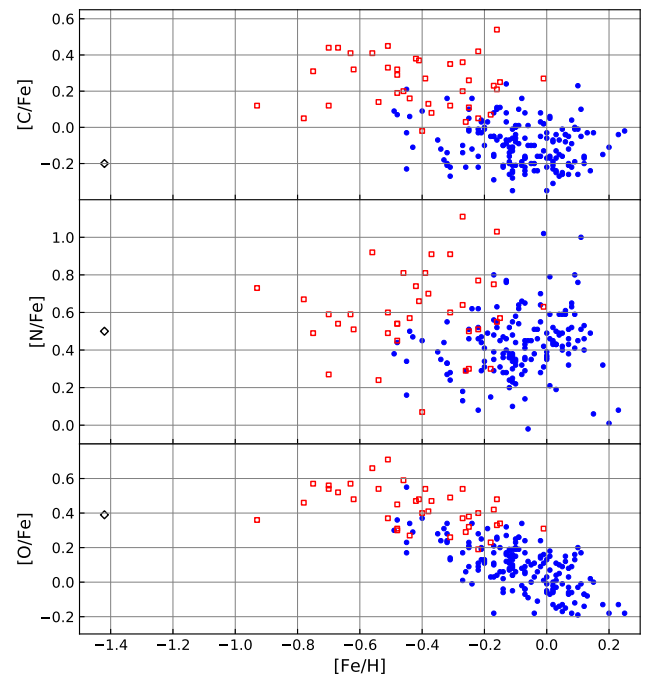


**Figure 7.** Observed carbon, nitrogen, and oxygen-to-iron element abundance ratios as a function of metallicity. The blue dots, red squares, and the black diamond represent the thin-disk, thick-disk, and halo stars, respectively.

### 3.2. Stellar Kinematic Properties, Ages, and Dependence to Galactic Subcomponents

The majority of the stars have radial velocities between  $-40$  and  $+20$   $\text{km s}^{-1}$ . We have compared our radial velocities with the *Gaia* DR2 catalog data. The mean and standard deviation of differences between the two sets is  $\langle \Delta V_{\text{rad}} \rangle = 0.05 \pm 0.53$   $\text{km s}^{-1}$ . Overall radial velocities and corresponding errors are presented in columns 11–12 of Table A1.

The ages of our sample stars are from about 1.0 to 11 Gyr; the majority are close to Solar, about

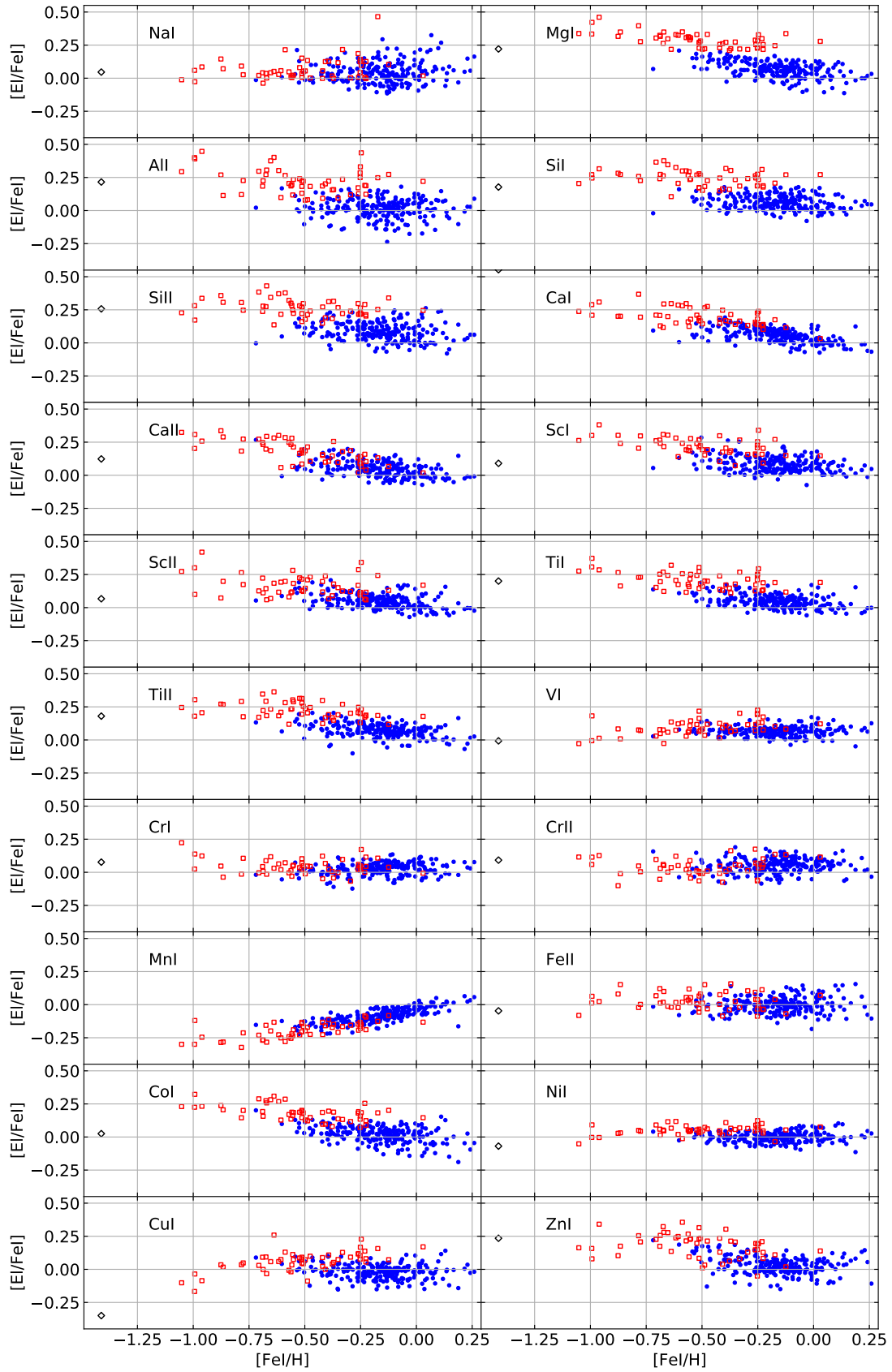
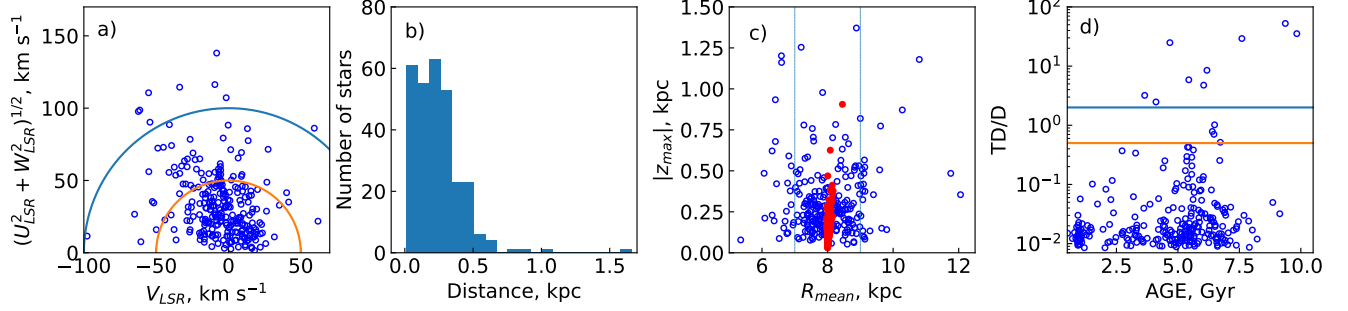
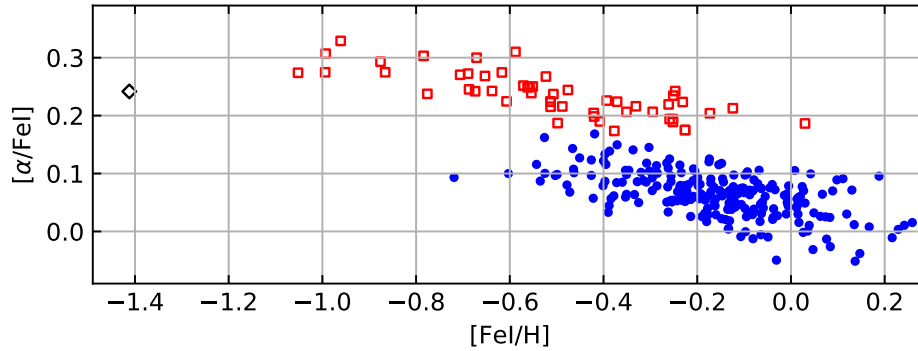


Figure 8. [E I/Fe I] ratios as a function of [Fe I/H]. The meaning of symbols as in Figure 7.





**Figure 9.** Kinematic parameters: (a) Toomre diagram of sample data with lines that show constant values of the total space velocity ( $v_{\text{tot}} = (U_{\text{LSR}} + V_{\text{LSR}} + W_{\text{LSR}})^{1/2}$ ) at 50 and 100  $\text{km s}^{-1}$ ; (b) histogram of distances of the sample stars; (c) distribution of the sample stars in a  $z_{\text{max}}$  versus  $R_{\text{mean}}$  plane, where the two vertical dashed lines delimit the Solar neighborhood  $7 < R_{\text{gc}} < 9$  kpc and the red circles are current positions ( $|z|$  vs.  $R$ ) for comparison; (d) kinematic thick-to-thin disk probability ratios (TD/D) vs. age for the sample stars, where the upper and lower lines mark TD/D=2.0 and TD/D=0.5, respectively.



**Figure 10.** Observed  $\alpha$ -to-iron element ratios as a function of  $[\text{Fe I}/\text{H}]$ .  $[\alpha/\text{Fe I}]$  is an average of Mg I, Si I, Si II, Ca I, Ca II, Ti I, and Ti II. The meaning of symbols as in Figure 7.

4 Gyr. The age values and uncertainties are presented in columns 13–14 of Table A1.

The  $U$ ,  $V$ , and  $W$  velocities; distances,  $R_{\text{mean}}$ ,  $z_{\text{max}}$ , and orbital eccentricities,  $e$ , with corresponding errors are presented in columns 15–27 of Table A1 and are exhibited in Figure 9.

It is widely accepted that Galactic subcomponents like thin and thick disks differ in a number of parameters. There are two widely used methods to separate them: kinematical (e.g. Bensby et al. 2003, 2005, 2014) and chemical (e.g. Adibekyan et al. 2012; Recio-Blanco et al. 2014).

The method introduced by Bensby et al. (2003, 2014) employs the thick-to-thin disk probability ratios. Stars with  $\text{TD/D} > 2$  are potential thick-disk stars, stars with  $\text{TD/D} < 0.5$  potentially belong to the thin disk, and stars with  $0.5 < \text{TD/D} < 2.0$  are called "in-between stars". Column 29 in Table A1 presents the thick-to-thin disk probability ratios ( $\text{TD/D}$ ). The panel (d) in Figure 9 displays the stellar  $\text{TD/D}$  distribution with age. According to the Toomre diagram (panel (d) in Figure 9), almost all our stars kinematically belong to the thin or thick disks except HD 175305 which according to Nissen & Schuster (2010) has a clear halo kinematics ( $(U_{\text{LSR}}^2 + W_{\text{LSR}}^2)^{1/2} = 290 \text{ km s}^{-1}$ ,  $V_{\text{LSR}} = -72 \text{ km s}^{-1}$ ,  $R_{\text{mean}} = 16 \text{ kpc}$ , and  $z_{\text{max}} = 20.6 \text{ kpc}$ ). Thus, using the kinematical method, we found that our sample consists of 262 thin-disk stars, nine thick-disk stars, and the remaining five stars are "in-between stars" and one halo star.

The chemical separation method can employ  $[\text{Mg I}/\text{Fe I}]$  (Adibekyan et al. 2012; Mikolaitis et al. 2014),  $[\text{Ti I}/\text{Fe I}]$  (Bensby et al. 2014), or  $[\alpha/\text{Fe I}]$  (Recio-Blanco et al. 2014) abundance ratios. As in our previous studies, we used  $[\text{Mg I}/\text{Fe I}]$  vs.  $[\text{Fe I}/\text{H}]$  to separate the low- $\alpha$  from high- $\alpha$  stars that potentially belong to the thin or thick disks, respectively. The most metal-poor star HD 175305 with halo kinematics should belong to the high- $\alpha$  halo population according to criteria by Nissen & Schuster (2010). Thus from chemical signatures, we revealed in our sample that there are 219 thindisk, 57 thick-disk, and one high- halo stars (column 83 in Table A1 presents stars were attributed to the thin or thick disks or a halo according to the chemical method).

In Figure 10 we show  $[\alpha/\text{Fe I}]$  which is an average of Mg I, Si I, Si II, Ca I, Ca II, Ti I, and Ti II (the  $[\alpha/\text{Fe I}]$  values and standard errors of the mean are presented in columns 81 and 82 of Table A1). The two disks are separated quite well. Exoplanets found near thin- and thick-disk stars will be of different chemical content.

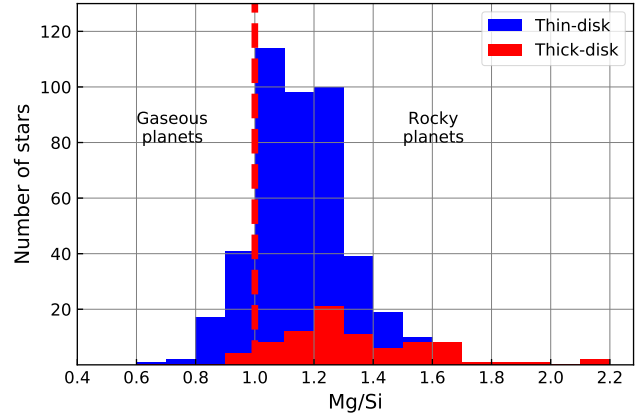


**Figure 11.** Distribution of Mg/Si ratio in thin- and thick-disk stars investigated in this work and M19. The vertical dashed line shows the approximate Si/Mg ratio, which separates stars potentially having gaseous and rocky planets, as suggested by e.g. Bond et al. 2010.

### 3.3. Stars as Potential Planet Hosts

The Mg/Si number ratio plays an important role in determining the plate tectonics and habitability of extra-solar planets. Theoretical studies have shown that if the Mg/Si number ratio is less than one, the extra-solar planet composition will be mostly made of pyroxene with other silicate based minerals, such as feldspar and a fraction of olivine (Bond et al. 2010). Furthermore, if the Mg/Si number ratio is between 1.0 and 2.0, as in our own planet Earth where  $\text{Mg}/\text{Si}_{\odot} = 1.05$ , the extra-solar planet composition will exist between pyroxene and olivine evenly. And lastly, if the Mg/Si number ratio is more than two, most of the planets will form from material with an olivine structure and the remaining magnesium will form oxides (Bond et al. 2010; Thiabaud et al. 2015). Thus, the planets originating from these three divisions would be different in term of plate tectonics, surface mineral chemistry, and inner geology.

Furthermore, Dorn et al. (2015) in their work concluded that in order to constrain the models for interior structure of rocky planets, the stellar chemical abundances, such as iron, silicon, and magnesium, are the key ingredients to reduce degeneracy in interior structure models and to constrain the mantle composition.

As suggested by, e.g. Bond et al. (2010) and Suárez-Andrés et al. (2018), the number ratio of  $\text{Mg}/\text{Si} = 1.0$  marks a division between stars that could form potentially gaseous or rocky planets. About 83% of our stars have Mg/Si values in the range between 1.0 and 2.0 with the mean value of  $\text{Mg}/\text{Si} = 1.18 \pm 0.13$ , which could suggest that they may have planets with a composition close to that of our planet Earth. The remaining  $\sim 17\%$  of the stars have  $\text{Mg}/\text{Si} \leq 1.0$ , where planets may have

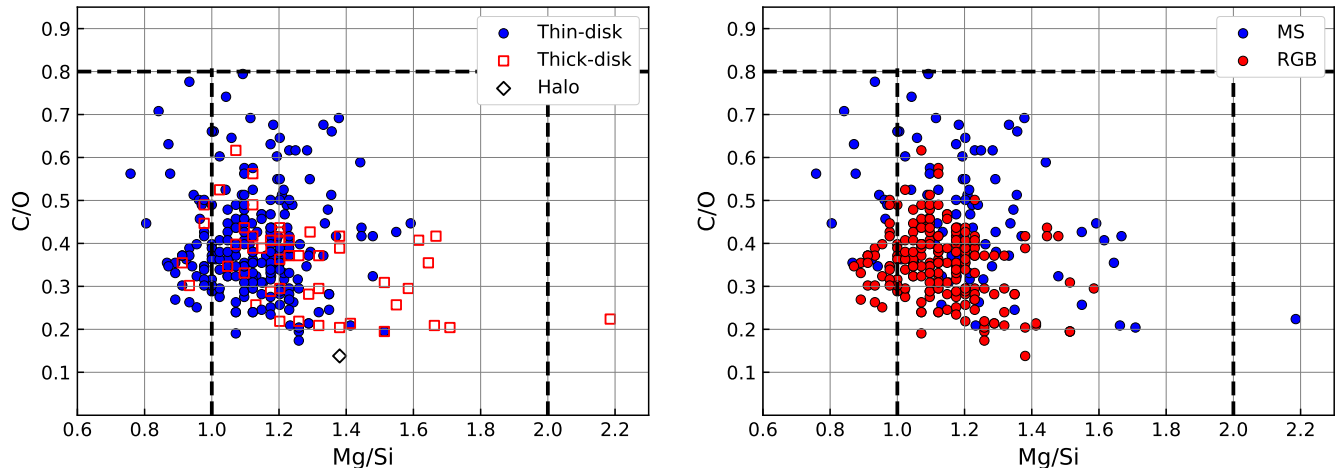


**Figure 12.**  $C/O$  number ratio as a function  $Mg/Si$  number ratio. On the left the colors and symbols represent the different Galactic components and on the right the stars are divided into the main-sequence and the red giant branch stars. Together with the data from this work, we plot 249 stars previously investigated with the same instrument and method of analysis (M19, Stonkutė et al. 2020).

a magnesium-depleted mineralogy. If we add to the sample of 277 stars investigated in this work and 249 stars investigated by M19 using the same instrument and method of analysis, the percentage of stars in the interval of  $1.0 < Mg/Si < 2.0$  increases by 1.4%. Suárez-Andrés et al. (2018) also found that  $\sim 83\%$  of their sample of 499 Solar-like stars to have a  $Mg/Si$  number ratio between 1.0 and 2.0, while Brewer & Fischer (2016) estimated a somewhat lower percentage among 847 investigated stars:  $\sim 64\%$ . The percentage of stars with the particular  $Mg/Si$  ratio may vary depending on how many stars belonging to the different Galactic subcomponents are in a sample. In Figure 11, we show a distribution of thin- and thick-disk stars according to their  $Mg/Si$  number ratios for the sample of 526 stars from our and M19 study.

In Figure 12, we also plotted the stars in the  $C/O$  versus  $Mg/Si$  number ratio diagrams. The left panel shows where stars are located according their dependence to the Galactic subcomponents, while in the right one, we can see how the  $C/O$  ratio differs in dwarfs and giants. Together with the data from this work, we plot 249 stars previously investigated with the same instrument and method of analysis (M19, Stonkutė et al. 2020). It can be seen that in giants, due to evolutionary changes of carbon, the  $C/O$  ratio, on average, is lower by about 0.1, thus we have to have in mind that planets that we find around evolved stars were formed when their host stars were young and had larger  $C/O$  ratios.

#### 4. SUMMARY

With the aim to contribute in fulfilling the primary goal of the ongoing NASA TESS mission – to char-

acterize planets around bright and nearby stars – in this paper, we present the main atmospheric parameters, ages, kinematic parameters, and abundances of 24 chemical elements determined from the high-resolution spectroscopy of all bright, ( $V < 8$  mag), slowly rotating, and cooler than F5 spectral type stars within the northern TESS CVZ. The observed TESS field also covers the CVZ of JWST, making the region particularly interesting for all types of astronomical studies.

In the northern TESS CVZ of an  $\sim 12$  degree radius, we observed all 302 stars with  $V < 8$  mag and  $(B - V) > 0.39$ , which roughly corresponds to  $T_{\text{eff}} < 6500$  K. Among them, 53 stars belong to the JWST CVZ as well.

There are 25 stars that appeared to be fast-rotating or double- or even triple-line systems so we decided to postpone for future analyses. A detailed characterization was done for a sample of 277 stars of different evolutionary stages, ages, and atmospheric parameters:  $T_{\text{eff}}$  varied between 3700 and 6600 K and  $[Fe/H]$  – between  $-1.5$  and  $0.25$  dex, ages – from 1 to 11 Gyr. A distinctive  $\log g$  distribution clearly separated giant and dwarf stars; the parameter of the former ones varied between 0.8 and 3.5, with a peak at 2.7, while the latter ones displayed values between 3.6 and 4.5 with a peak at 4.3. Data from the *Gaia* DR2 catalog was used to calculate stellar kinematic parameters; the mean Galactocentric distances,  $R_{\text{mean}}$ , span from 5 to 12 kpc and distances from the Galactic plane,  $z_{\text{max}}$ , reach 1.5 kpc. Stellar velocity components ( $U$ ,  $V$ , and  $W$ ) were determined as well.

Along with the main atmospheric parameters, abundances of the 24 chemical species determined will serve for the detailed characterization of exoplanets, if discov-

ered around the investigated stars by the NASA TESS space telescope, for the interpretation of exoplanet atmospheres to be made by the upcoming NASA JWST mission and in answering many stellar and Galactic evolution questions. The vast majority of our sample stars ( $\sim 83\%$ ) exhibit Mg/Si ratios greater than 1.0 and may potentially harbor rocky planets in their systems.

Only around one third of bright  $V < 8$  mag stars have spectroscopic observations in the literature. This fact is evident from the star sample of this study as well. Out of 277 stars selected for the spectroscopic analysis, only 47 had previously derived atmospheric parameters from high-resolution spectroscopy. In the era of exoplanet search among bright stars, this gap of study is more significant than ever, since knowledge of precise stellar

atmospheric parameters are very important in characterizing exoplanets and stars themselves.

We acknowledge the grant from the European Social Fund via the Lithuanian Science Council (LMTLT) grant No. 09.3.3-LMT-K-712-01-0103. We thank the anonymous referee for a constructive report that helped to improved this paper. We have made extensive use of the NASA ADS and SIMBAD databases. We are grateful to the Moletai Astronomical Observatory of Vilnius University for providing observing time for this project.

*Facility:* Exoplanet Archive.

*Software:* Astropy (Astropy Collaboration et al. 2018), DAOSPEC (Stetson & Pancino 2008), MOOG (Snedden 1973), galpy (Bovy 2015), TURBOSPECTRUM (Alvarez & Plez 1998), UniDAM (Mints & Hekker 2017).

## APPENDIX

### A. APPENDIX INFORMATION

Table A1 lists the contents of the Machine-readable table (atmospheric parameters, kinematic properties, ages, and individual abundances) together with associated errors, and other information for the investigated stars.

**Table A1.** Contents of the Machine-readable Table

Col	Label	Units	Explanations
1	ID	—	Tycho catalog identification
2	TESS_ID	—	ID in the TESS catalog
3	Teff	K	Effective temperature
4	eTeff	K	Error on effective temperature
5	Logg	dex	Surface gravity
6	e_Logg	dex	Error on surface gravity
7	[Fe/H]	dex	Metallicity
8	e_[Fe/H]	dex	Error on metallicity
9	Vt	km s <sup>-1</sup>	Microturbulence velocity
10	e_Vt	km s <sup>-1</sup>	Error on microturbulence velocity
11	Vrad	km s <sup>-1</sup>	Radial velocity
12	e_Vrad	km s <sup>-1</sup>	Error on radial velocity
13	Age	log(yr)	Log age of the star
14	e_Age	log(yr)	Error on log Age
15	U	km s <sup>-1</sup>	$U$ velocity
16	e_U	km s <sup>-1</sup>	Error on $U$ velocity
17	V	km s <sup>-1</sup>	$V$ velocity
18	e_V	km s <sup>-1</sup>	Error on $V$ velocity
19	W	km s <sup>-1</sup>	$W$ velocity
20	e_W	km s <sup>-1</sup>	Error on $W$ velocity
21	d	kpc	Distance calculated 1/plx
22	R <sub>mean</sub>	kpc	Mean Galactocentric distance
23	e_R <sub>mean</sub>	kpc	Error on mean Galactocentric distance

24	$z_{max}$	kpc	Distance from Galactic plane
25	$e_{z_{max}}$	kpc	Error on distance from Galactic plane
26	$e$	—	Orbital eccentricity
27	$e_e$	—	Error on orbital eccentricity
28	TD/D	—	Thick-to-thin disk probability ratio
29	[C/H]	dex	Carbon abundance
30	$e_{[C/H]}$	dex	Error on carbon abundance
...			
75	[Zn I/H]	dex	Zinc abundance
76	$e_{[Zn I/H]}$	dex	Error on zinc abundance
77	[Fe I/H]	dex	Iron abundance
78	$e_{[Fe I/H]}$	dex	Error on iron abundance
79	[Fe II/H]	dex	Ionized iron abundance
80	$e_{[Fe II/H]}$	dex	Error on ionized iron abundance
81	[alpha/Fe I]	dex	Averaged Mg I, Si I, Si II, Ca I, Ca II, Ti I, and Ti II to Fe I abundance ratio
82	$e_{[alpha/Fe I]}$	dex	Standard error of the mean on [alpha/Fe I]
83	Group	—	Chemical attribution to the Galactic subcomponent

## REFERENCES

- Adamczak, J., & Lambert, D. L. 2014, ApJ, 791, 58, doi: [10.1088/0004-637X/791/1/58](https://doi.org/10.1088/0004-637X/791/1/58)
- Adibekyan, V. Z., Sousa, S. G., Santos, N. C., et al. 2012, A&A, 545, A32, doi: [10.1051/0004-6361/201219401](https://doi.org/10.1051/0004-6361/201219401)
- Afşar, M., Sneden, C., & For, B. Q. 2012, AJ, 144, 20, doi: [10.1088/0004-6256/144/1/20](https://doi.org/10.1088/0004-6256/144/1/20)
- Aguilera-Gómez, C., Ramírez, I., & Chanamé, J. 2018, A&A, 614, A55, doi: [10.1051/0004-6361/201732209](https://doi.org/10.1051/0004-6361/201732209)
- Ahumada, R., Allende Prieto, C., Almeida, A., et al. 2019, arXiv e-prints, arXiv:1912.02905, <https://arxiv.org/abs/1912.02905>
- Akeson, R. L., Chen, X., Ciardi, D., et al. 2013, PASP, 125, 989, doi: [10.1086/672273](https://doi.org/10.1086/672273)
- Alvarez, R., & Plez, B. 1998, A&A, 330, 1109
- Andrae, R., Fouesneau, M., Creevey, O., et al. 2018, A&A, 616, A8, doi: [10.1051/0004-6361/201732516](https://doi.org/10.1051/0004-6361/201732516)
- Astropy Collaboration, Price-Whelan, A. M., Sipőcz, B. M., et al. 2018, AJ, 156, 123, doi: [10.3847/1538-3881/aabc4f](https://doi.org/10.3847/1538-3881/aabc4f)
- Barclay, T., Pepper, J., & Quintana, E. V. 2018, ApJS, 239, 2, doi: [10.3847/1538-4365/aae3e9](https://doi.org/10.3847/1538-4365/aae3e9)
- Bensby, T., Feltzing, S., & Lundström, I. 2003, A&A, 410, 527, doi: [10.1051/0004-6361:20031213](https://doi.org/10.1051/0004-6361:20031213)
- Bensby, T., Feltzing, S., Lundström, I., & Ilyin, I. 2005, A&A, 433, 185, doi: [10.1051/0004-6361:20040332](https://doi.org/10.1051/0004-6361:20040332)
- Bensby, T., Feltzing, S., & Oey, M. S. 2014, A&A, 562, A71, doi: [10.1051/0004-6361/201322631](https://doi.org/10.1051/0004-6361/201322631)
- Bitsch, B., & Battistini, C. 2020, A&A, 633, A10, doi: [10.1051/0004-6361/201936463](https://doi.org/10.1051/0004-6361/201936463)
- Bond, J. C., O'Brien, D. P., & Lauretta, D. S. 2010, ApJ, 715, 1050, doi: [10.1088/0004-637X/715/2/1050](https://doi.org/10.1088/0004-637X/715/2/1050)
- Borucki, W. J., Koch, D., Basri, G., et al. 2010, Science, 327, 977, doi: [10.1126/science.1185402](https://doi.org/10.1126/science.1185402)
- Bovy, J. 2015, ApJS, 216, 29, doi: [10.1088/0067-0049/216/2/29](https://doi.org/10.1088/0067-0049/216/2/29)
- Bovy, J., Allende Prieto, C., Beers, T. C., et al. 2012, ApJ, 759, 131, doi: [10.1088/0004-637X/759/2/131](https://doi.org/10.1088/0004-637X/759/2/131)
- Bressan, A., Marigo, P., Girardi, L., et al. 2012, MNRAS, 427, 127, doi: [10.1111/j.1365-2966.2012.21948.x](https://doi.org/10.1111/j.1365-2966.2012.21948.x)
- Brewer, J. M., & Fischer, D. A. 2016, ApJ, 831, 20, doi: [10.3847/0004-637X/831/1/20](https://doi.org/10.3847/0004-637X/831/1/20)
- Brewer, J. M., Fischer, D. A., Valenti, J. A., & Piskunov, N. 2016, ApJS, 225, 32, doi: [10.3847/0067-0049/225/2/32](https://doi.org/10.3847/0067-0049/225/2/32)
- Britavskiy, N. E., Andrievsky, S. M., Tsymbal, V. V., et al. 2012, A&A, 542, A104, doi: [10.1051/0004-6361/201118297](https://doi.org/10.1051/0004-6361/201118297)
- Brooke, J. S. A., Bernath, P. F., Schmidt, T. W., & Bacsakay, G. B. 2013, JQSRT, 124, 11, doi: [10.1016/j.jqsrt.2013.02.025](https://doi.org/10.1016/j.jqsrt.2013.02.025)
- Cabral, N., Lagarde, N., Reylé, C., Guilbert-Lepoutre, A., & Robin, A. C. 2019, A&A, 622, A49, doi: [10.1051/0004-6361/201833750](https://doi.org/10.1051/0004-6361/201833750)
- Cutri, R. M., & et al. 2014, VizieR Online Data Catalog, II/328
- da Silva, R., Milone, A. C., & Reddy, B. E. 2011, A&A, 526, A71, doi: [10.1051/0004-6361/201015907](https://doi.org/10.1051/0004-6361/201015907)



- da Silva, R., Milone, A. d. C., & Rocha-Pinto, H. J. 2015, *A&A*, 580, A24, doi: [10.1051/0004-6361/201525770](https://doi.org/10.1051/0004-6361/201525770)
- Deka-Szymankiewicz, B., Niedzielski, A., Adamczyk, M., et al. 2018, *A&A*, 615, A31, doi: [10.1051/0004-6361/201731696](https://doi.org/10.1051/0004-6361/201731696)
- Dorn, C., Khan, A., Heng, K., et al. 2015, *A&A*, 577, A83, doi: [10.1051/0004-6361/201424915](https://doi.org/10.1051/0004-6361/201424915)
- Dulick, M., Bauschlicher, Jr., C. W., Burrows, A., et al. 2003, *ApJ*, 594, 651, doi: [10.1086/376791](https://doi.org/10.1086/376791)
- García Pérez, A. E., Allende Prieto, C., Holtzman, J. A., et al. 2016, *AJ*, 151, 144, doi: [10.3847/0004-6256/151/6/144](https://doi.org/10.3847/0004-6256/151/6/144)
- Gardner, J. P., Mather, J. C., Clampin, M., et al. 2006, *SSRv*, 123, 485, doi: [10.1007/s11214-006-8315-7](https://doi.org/10.1007/s11214-006-8315-7)
- Grevesse, N., Asplund, M., & Sauval, A. J. 2007, *SSRv*, 130, 105, doi: [10.1007/s11214-007-9173-7](https://doi.org/10.1007/s11214-007-9173-7)
- Gustafsson, B., Edvardsson, B., Eriksson, K., et al. 2008, *A&A*, 486, 951, doi: [10.1051/0004-6361:200809724](https://doi.org/10.1051/0004-6361:200809724)
- Heiter, U., Lind, K., Asplund, M., et al. 2015, *PhyS*, 90, 054010, doi: [10.1088/0031-8949/90/5/054010](https://doi.org/10.1088/0031-8949/90/5/054010)
- Hekker, S., & Meléndez, J. 2007, *A&A*, 475, 1003, doi: [10.1051/0004-6361:20078233](https://doi.org/10.1051/0004-6361:20078233)
- Jönsson, H., Ryde, N., Nordlander, T., et al. 2017, *A&A*, 598, A100, doi: [10.1051/0004-6361/201629128](https://doi.org/10.1051/0004-6361/201629128)
- Joshi, Y. C. 2007, *MNRAS*, 378, 768, doi: [10.1111/j.1365-2966.2007.11831.x](https://doi.org/10.1111/j.1365-2966.2007.11831.x)
- Jurgenson, C., Fischer, D., McCracken, T., et al. 2016, *Journal of Astronomical Instrumentation*, 5, 1650003, doi: [10.1142/S2251171716500033](https://doi.org/10.1142/S2251171716500033)
- Katz, D., Sartoretti, P., Cropper, M., et al. 2019, *A&A*, 622, A205, doi: [10.1051/0004-6361/201833273](https://doi.org/10.1051/0004-6361/201833273)
- Kempton, E. M. R., Bean, J. L., Louie, D. R., et al. 2018, *PASP*, 130, 114401, doi: [10.1088/1538-3873/aadf6f](https://doi.org/10.1088/1538-3873/aadf6f)
- Koch, D. G., Borucki, W. J., Basri, G., et al. 2010, *ApJL*, 713, L79, doi: [10.1088/2041-8205/713/2/L79](https://doi.org/10.1088/2041-8205/713/2/L79)
- Kurucz, R. 1993, *Diatomic Molecular Data for Opacity Calculations*. Kurucz CD-ROM No. 15. Cambridge, Mass.: Smithsonian Astrophysical Observatory, 1993., 15
- Lambert, D. L., Gustafsson, B., Eriksson, K., & Hinkle, K. H. 1986, *ApJS*, 62, 373, doi: [10.1086/191145](https://doi.org/10.1086/191145)
- Lee, Y. S., Beers, T. C., Allende Prieto, C., et al. 2011, *AJ*, 141, 90, doi: [10.1088/0004-6256/141/3/90](https://doi.org/10.1088/0004-6256/141/3/90)
- Liu, Y. J., Tan, K. F., Wang, L., et al. 2014, *ApJ*, 785, 94, doi: [10.1088/0004-637X/785/2/94](https://doi.org/10.1088/0004-637X/785/2/94)
- Luck, R. E. 2017, *AJ*, 153, 21, doi: [10.3847/1538-3881/153/1/21](https://doi.org/10.3847/1538-3881/153/1/21)
- Luck, R. E., & Heiter, U. 2007, *AJ*, 133, 2464, doi: [10.1086/513194](https://doi.org/10.1086/513194)
- Luri, X., Brown, A. G. A., Sarro, L. M., et al. 2018, *A&A*, 616, A9, doi: [10.1051/0004-6361/201832964](https://doi.org/10.1051/0004-6361/201832964)
- Maldonado, J., & Villaver, E. 2016, *A&A*, 588, A98, doi: [10.1051/0004-6361/201527883](https://doi.org/10.1051/0004-6361/201527883)
- Masseron, T., Plez, B., Van Eck, S., et al. 2014, *A&A*, 571, A47, doi: [10.1051/0004-6361/201423956](https://doi.org/10.1051/0004-6361/201423956)
- McWilliam, A. 1990, *ApJS*, 74, 1075, doi: [10.1086/191527](https://doi.org/10.1086/191527)
- Mikolaitis, Š., Tautvaišienė, G., Drazdauskas, A., et al. 2018, *PASP*, 130, 074202, doi: [10.1088/1538-3873/aabfb6](https://doi.org/10.1088/1538-3873/aabfb6)
- Mikolaitis, Š., Hill, V., Recio-Blanco, A., et al. 2014, *A&A*, 572, A33, doi: [10.1051/0004-6361/201424093](https://doi.org/10.1051/0004-6361/201424093)
- Mikolaitis, Š., Drazdauskas, A., Minkevičiūtė, R., et al. 2019, *A&A*, 628, A49, doi: [10.1051/0004-6361/201835004](https://doi.org/10.1051/0004-6361/201835004)
- Mints, A., & Hekker, S. 2017, *A&A*, 604, A108, doi: [10.1051/0004-6361/201630090](https://doi.org/10.1051/0004-6361/201630090)
- Nissen, P. E., & Schuster, W. J. 2010, *A&A*, 511, L10, doi: [10.1051/0004-6361/200913877](https://doi.org/10.1051/0004-6361/200913877)
- Nordström, B., Mayor, M., Andersen, J., et al. 2004, *A&A*, 418, 989, doi: [10.1051/0004-6361:20035959](https://doi.org/10.1051/0004-6361:20035959)
- Pompéia, L., Masseron, T., Famaey, B., et al. 2011, *MNRAS*, 415, 1138, doi: [10.1111/j.1365-2966.2011.18685.x](https://doi.org/10.1111/j.1365-2966.2011.18685.x)
- Ram, R. S., Brooke, J. S. A., Bernath, P. F., Sneden, C., & Lucatello, S. 2014, *ApJS*, 211, 5, doi: [10.1088/0067-0049/211/1/5](https://doi.org/10.1088/0067-0049/211/1/5)
- Rauer, H., Aerts, C., Cabrera, J., & PLATO Team. 2016, *Astronomische Nachrichten*, 337, 961, doi: [10.1002/asna.201612408](https://doi.org/10.1002/asna.201612408)
- Rauer, H., Catala, C., Aerts, C., et al. 2014, *Experimental Astronomy*, 38, 249, doi: [10.1007/s10686-014-9383-4](https://doi.org/10.1007/s10686-014-9383-4)
- Recio-Blanco, A., de Laverny, P., Kordopatis, G., et al. 2014, *A&A*, 567, A5, doi: [10.1051/0004-6361/201322944](https://doi.org/10.1051/0004-6361/201322944)
- Ricker, G. R., Winn, J. N., Vanderspek, R., et al. 2015, *Journal of Astronomical Telescopes, Instruments, and Systems*, 1, 014003, doi: [10.1117/1.JATIS.1.1.014003](https://doi.org/10.1117/1.JATIS.1.1.014003)
- Roederer, I. U., Preston, G. W., Thompson, I. B., et al. 2014, *AJ*, 147, 136, doi: [10.1088/0004-6256/147/6/136](https://doi.org/10.1088/0004-6256/147/6/136)
- Santos, N. C., Adibekyan, V., Dorn, C., et al. 2017, *A&A*, 608, A94, doi: [10.1051/0004-6361/201731359](https://doi.org/10.1051/0004-6361/201731359)
- Schönrich, R., Binney, J., & Dehnen, W. 2010, *MNRAS*, 403, 1829, doi: [10.1111/j.1365-2966.2010.16253.x](https://doi.org/10.1111/j.1365-2966.2010.16253.x)
- Skrutskie, M. F., Cutri, R. M., Stiening, R., et al. 2006, *AJ*, 131, 1163, doi: [10.1086/498708](https://doi.org/10.1086/498708)
- Smiljanic, R., Korn, A. J., Bergemann, M., et al. 2014, *A&A*, 570, A122, doi: [10.1051/0004-6361/201423937](https://doi.org/10.1051/0004-6361/201423937)
- Smith, V. V., Cunha, K., Shetrone, M. D., et al. 2013, *ApJ*, 765, 16, doi: [10.1088/0004-637X/765/1/16](https://doi.org/10.1088/0004-637X/765/1/16)
- Sneden, C., Lucatello, S., Ram, R. S., Brooke, J. S. A., & Bernath, P. 2014, *ApJS*, 214, 26, doi: [10.1088/0067-0049/214/2/26](https://doi.org/10.1088/0067-0049/214/2/26)
- Sneden, C. A. 1973, PhD thesis, THE UNIVERSITY OF TEXAS AT AUSTIN.

- Soubiran, C., Le Campion, J.-F., Cayrel de Strobel, G., & Caillo, A. 2010, *A&A*, 515, A111, doi: [10.1051/0004-6361/201014247](https://doi.org/10.1051/0004-6361/201014247)
- Stassun, K. G., Oelkers, R. J., Pepper, J., et al. 2018, *AJ*, 156, 102, doi: [10.3847/1538-3881/aad050](https://doi.org/10.3847/1538-3881/aad050)
- Stetson, P. B., & Pancino, E. 2008, *PASP*, 120, 1332, doi: [10.1086/596126](https://doi.org/10.1086/596126)
- Stonkutė, E., Chorniy, Y., Tautvaišienė, G., et al. 2020, *AJ*, 159, 90, doi: [10.3847/1538-3881/ab6a19](https://doi.org/10.3847/1538-3881/ab6a19)
- Suárez-Andrés, L., Israelian, G., González Hernández, J. I., et al. 2018, *A&A*, 614, A84, doi: [10.1051/0004-6361/201730743](https://doi.org/10.1051/0004-6361/201730743)
- Thiabaud, A., Marboeuf, U., Alibert, Y., Laya, I., & Mezger, K. 2015, *A&A*, 580, A30, doi: [10.1051/0004-6361/201525963](https://doi.org/10.1051/0004-6361/201525963)
- Thompson, S. E., Coughlin, J. L., Hoffman, K., et al. 2018, *ApJS*, 235, 38, doi: [10.3847/1538-4365/aab4f9](https://doi.org/10.3847/1538-4365/aab4f9)
- Wenger, M., Ochsenbein, F., Egret, D., et al. 2000, *A&AS*, 143, 9, doi: [10.1051/aas:2000332](https://doi.org/10.1051/aas:2000332)